Lagrangian structures and mixing in the wake of a streamwise oscillating cylinder

N. Cagney[1,a] and S. Balabani[2,b]

[1]*Department of Earth Sciences, University College London, Gower Street, London WC1E 6BT, United Kingdom*
[2]*Department of Mechanical Engineering, University College London, Gower Street, London WC1E 7JE, United Kingdom*

Lagrangian analysis is capable of revealing the underlying structure and complex phenomena in unsteady flows. We present particle-image velocimetry measurements of the wake of a cylinder undergoing streamwise vortex-induced vibrations and calculate the Finite-Time Lyapunov Exponents (FTLE) in backward- and forward-time. The FTLE fields are compared to the phase-averaged vorticity fields for the four different wake modes observed while the cylinder experiences streamwise vortex-induced vibrations. The backward-time FTLE fields characterise the formation of vortices, with the roll up of spiral-shaped ridges coinciding with the roll up of the shear layers to form the vortices. Ridges in the forward-time fields tend to lie perpendicular to the flow direction and separate nearby vortices. The shedding of vortices coincides with a "peel off" process in the forward-time FTLE fields, in which a ridge connected to the cylinder splits into two strips, one of which moves downstream. Particular attention is given to the "wake breathing" process, in which the streamwise motion of the cylinder causes both shear layers to roll up simultaneously and two vortices of opposite sign to be shed into the wake. In this case, the ridges in forward-time FTLE fields are shown to define "vortex cells," in which the new vortices form, and the FTLE fields allow the wake to be decomposed into three distinct regions. Finally, the mixing associated with each wake mode is examined, and it is shown that cross-wake mixing is significantly enhanced when the vibration amplitude is large and the vortices are shed alternately. However, while the symmetric shedding induces large amplitude vibrations, no increase in mixing is observed relative to the von Kármán vortex street observed behind near-stationary bodies. © *2016 Author(s). All article content, except where otherwise noted, is licensed under a Creative Commons Attribution 3.0 Unported License.* [http://dx.doi.org/10.1063/1.4945784]

I. INTRODUCTION

Flow past a cylinder is a classical case of unsteady fluid-structure interaction, with the shear layers on either sides of the cylinder rolling up periodically to form vortices that are then shed downstream. The vortices in the wake arrange into a characteristic pattern known as the von Kármán vortex street, which has been seen in small scale flow-visualisation experiments[1] as well as on very large scales, including the wakes around islands and mountains.[2,3] The shedding process results in very interesting Lagrangian dynamics, which have been examined in detail using an unsteady potential flow model,[4] demonstrating the presence of chaos in the near wake.[5] The presence of chaotic advection significantly increases mixing efficiency,[6,7] which has been examined with respect to chemical reactions[5] and the mixing in ocean flows around islands.[8]

---

a)Electronic mail: neil.cagney.11@ucl.ac.uk
b)Electronic mail: s.balabani@ucl.ac.uk

    28, 000000-1

PROOF COPY [15-1670A] 022604PHF

000000-2   N. Cagney and S. Balabani   Phys. Fluids **28**, 000000 (2016)

The latter problem was investigated by Crimaldi and Kawakami,[9,10] who performed numerical simulations of steady flow past a stationary cylinder to investigate the mixing of passive tracers, and how this may affect the fertilisation of the eggs of marine species near islands.

There has been relatively little experimental work investigating the Lagrangian dynamics in cylinder wakes. Bourgeois *et al.*[11] examined the three-dimensional Lagrangian structures in the wake of a square cylinder attached to a plate using the Finite-Time Lyapunov Exponent (FTLE) fields, which represent the local rate of fluid stretching and are often used to approximate the Lagrangian Coherent Structures (LCSs).[12] Using the FTLE fields, they were able to characterise the influence of the plate on the three-dimensional shedding process. Similarly, Kourentis and Konstantinidis[13] used a combination of proper-orthogonal decomposition and the FTLE fields to identify the effect of flow pulsations on the structures in the near wake of a circular cylinder and used the resulting approximations of the LCSs to derive measures of the width and decay of the wake pattern.
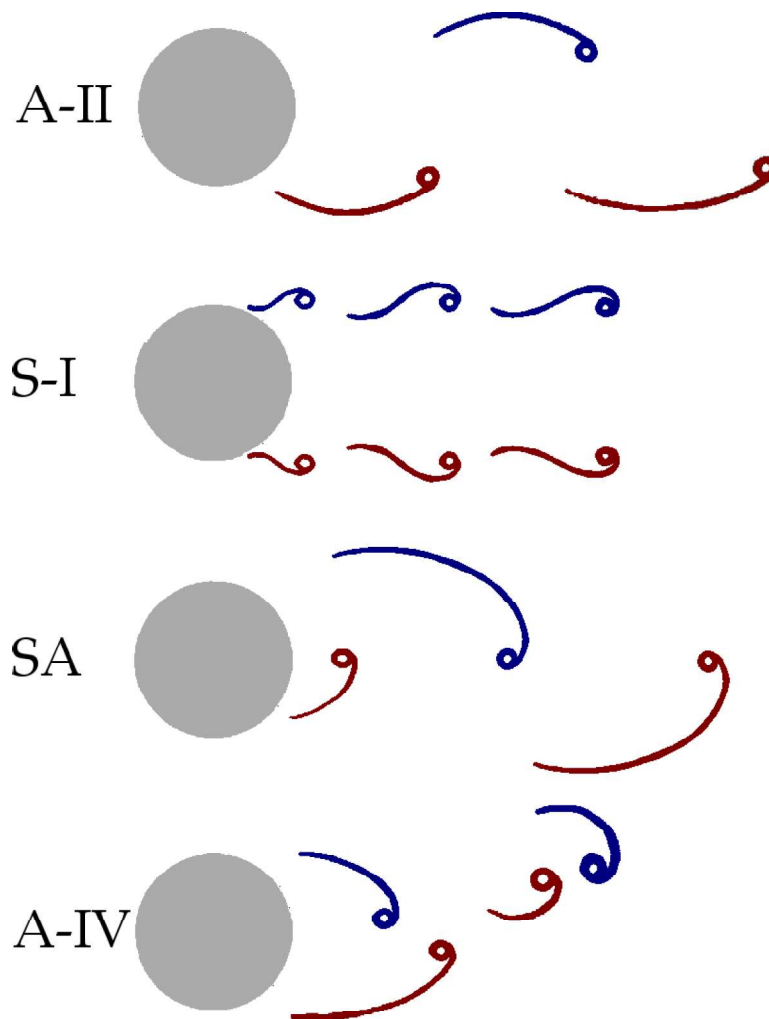
Celik and Beskok[14] examined the flow of passive tracers past a cylinder in a channel and showed that the mixing in the cylinder wake is significantly enhanced if the cylinder is forced to oscillate transverse to the flow direction. This has the potential for interesting new dynamics, given the wide range of patterns of vortices, or "wake modes," that can occur, depending on the non-dimensional oscillation amplitude, A/D, and frequency, $f_x D/U_0$ (where D and U_0 are the cylinder diameter and freestream velocity, respectively).[15–17]

The unsteady wake dynamics are capable of causing the cylinder to oscillate in the absence of external forcing. The vortices are shed at a fixed frequency, f_{St}, given by the Strouhal number, $St = f_{St}D/U_0$; this can lead to Vortex-Induced Vibrations (VIVs) if the frequency of the fluid forces induced by the shedding process coincides with the natural frequency of the cylinder, f_n, or its actual vibration frequency, f_x, which may be slightly different due to added mass effects. These vibrations can reach large amplitudes and cause significant fatigue damage.[18] The condition for VIV is given by the "true" reduced velocity, $U_r St/f^*$, where $U_r = U_0/f_n D$ is the conventional reduced velocity and $f^* = f_x/f_n$ is the frequency ratio. The "true" reduced velocity (henceforth referred to simply as the reduced velocity) is equal to the ratio of the predicted shedding frequency to the vibration frequency, f_{St}/f_x. VIV typically occurs in the transverse (lift) direction at $U_r St/f^* \approx 1$; however, as the unsteady drag force typically occurs at twice the shedding frequency, VIV occurs at $U_r St/f^* \approx 0.5$ in the streamwise (drag) direction.

The vibration amplitudes tend to be smaller in the streamwise direction compared to the transverse;[19,20] however, streamwise VIV is also relevant to the study of stationary cylinders experiencing wave-loading or in pulsatile flow, as occurs in blood flow, tidal flows and various industrial contexts. Provided that the amplitude of the pulsations is low, the case of a cylinder freely oscillating in the streamwise direction in steady flow is dynamically equivalent to a fixed cylinder in pulsating flow.[21,22]

For streamwise VIV of a circular cylinder, four wake modes have been observed, which are shown in Figure 1, and the response regime is characterised by two branches, separated by a region of low amplitude vibration at resonance, i.e., $U_r St/f^* \approx 0.5$. When the vibration amplitude, A, of the cylinder is low the A-II mode occurs,[23–25] which is essentially the von Kármán vortex street seen behind stationary cylinders (Figure 1). The first response branch occurs over the range $U_r St/f^* \approx 0.25$–0.45 and is characterised by the presence of the S-I mode, in which two vortices of opposite sign are shed simultaneously from either sides of the cylinder[23,24,26,27] (Figure 1). This symmetric shedding is apparently unique to bodies experiencing streamwise VIV or periodic wave loading. Naudascher[26] described the process in detail (based on the work of Aguirre[23]); the streamwise motion of the cylinder causes the shear layers on either sides of the cylinder to roll up simultaneously, in a process he referred to as "wake breathing." The symmetric arrangement is unstable and tends to rearrange downstream into an alternate pattern.[28,29] Aguirre showed that the wake reverts to the A-II mode at the peak of the first branch, which was also observed by the present authors.[24,30]

The vibration amplitude is low at resonance, $U_r St/f^* \approx 0.5$. The reason for this counterintuitive reduction in amplitude is not clear; previous authors have argued that it arises from a change in the wake mode,[23] a change in the phase of vortex-shedding with respect to the cylinder motion[22] or a reduction in the amplitude of the fluid forces.[31] As the reduced velocity is

PROOF COPY [15-1670A] 022604PHF

000000-3   N. Cagney and S. Balabani   Phys. Fluids **28**, 000000 (2016)

FIG. 1. Sketch showing the various wakes observed for streamwise VIV.

increased further, the vibration amplitude recovers to form the second response branch in the range $U_rSt/f^* \approx 0.55$–0.65, which is characterised by the SA mode.[27] This is a special case of the A-II mode, in which the vortices form very close to the cylinder, have a greater circulation, and remain close to the wake centreline as they convect downstream[24] (Figure 1).

The A-IV mode has been observed in studies in which a cylinder is forced to oscillate[17,25] or is placed in pulsating flow.[32] This mode is characterised by the shedding of four vortices per wake cycle, with a pair of counter-rotating vortices shed in each cylinder oscillation cycle (Figure 1), and has recently been shown to also occur in the wake of freely oscillating cylinders in the second response branch,[33] using the same experimental data presented in this paper.

Wake modes are typically identified in flow-visualisation studies using dye[1,25,34] or laser-induced fluorescence.[17] When the velocity fields in the wake are measured, the wake mode can also be identified from the vorticity fields,[15,24,27,35] although in practice it can be difficult to distinguish vortices in the near wake due to the high shear surrounding the cylinder. This can be mitigated by using various Eulerian measures to identify coherent vortices, such as the Δ, λ, and Q criteria which are derived from a decomposition of the local velocity gradient tensor.[36–38] While these Eulerian measures can be extremely useful, they suffer some drawbacks:[37,38] they typically require a user-defined threshold and therefore the identified boundaries of vortices are subjective, and they do not contain any information on the history of the flow. An alternative approach that overcomes these issues is to identify the wake mode and the Lagrangian structures from the FTLE fields computed in

forward- and backward-time, which correspond to the repelling and attracting structures in the flow, respectively. This approach is often used to approximate the LCSs and is capable of revealing the complex processes governing flows,[12,39,40] identifying regions of strong or weak mixing,[38,41] as well as producing strikingly beautiful visualisations.[42]

This paper aims to provide new insight into the dynamics and Lagrangian structures associated with the various wake modes observed in streamwise VIV and to investigate their effect on fluid mixing. The remainder of the paper is structured as follows; Section II describes the experimental system and the Lagrangian calculations; Section III summarises the response regime of the streamwise oscillating cylinder, describes the FTLE fields observed for wake mode and discusses their relationship to the vortex dynamics; the wake modes are examined in terms of their mixing characteristics in Section IV; and finally some concluding remarks are made in Section V.

II. EXPERIMENTAL DETAILS

The experiments were performed in a closed-loop water tunnel, which has been described previously by Konstantinidis *et al.*[21] The test-section had internal dimensions of 72 mm × 72 mm and was positioned downstream of a 9:1 contraction and honeycomb screens, such that the turbulence entering the test-section was less than 2%. A cooling system was used to ensure that the temperature was held constant at 22 ± 0.5 °C.

A cylinder was supported within the test-section using fishing wires, such that it was free to vibrate only in the streamwise direction, as shown in Figure 2. The tension in each wire was adjusted, and tests were performed to ensure that any non-streamwise motion (i.e., pitching) that the cylinder experienced was negligible. The cylinder had a diameter of 7.1 mm and was 71 mm in length. It was made of solid perspex and had a mass ratio (i.e., the ratio of the cylinder mass to the displaced fluid mass) of 1.17. A series of tap tests were performed in air and water; the natural frequency in water was $f_n = 23.7$ Hz, and the structural damping ratio (measured in air) was 0.0037. The damping ratio increased to 0.02 when the tests were performed in water, i.e., when the effects of hydrodynamic damping were included.
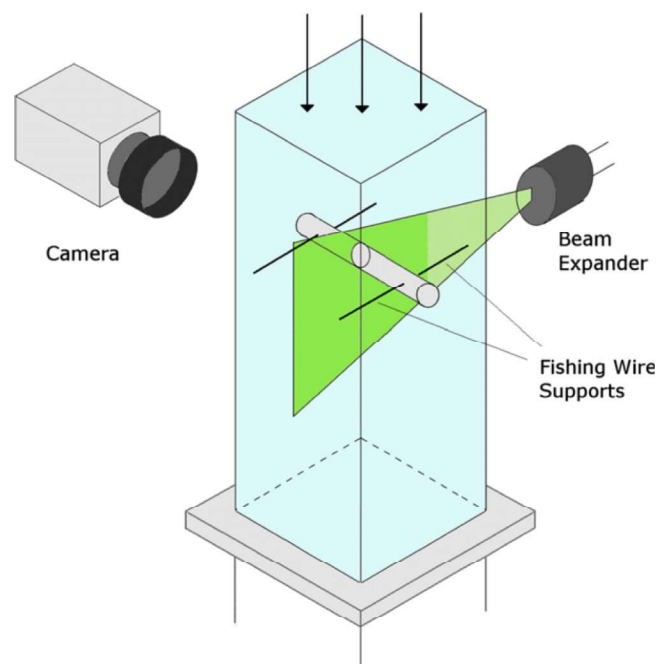

FIG. 2. Sketch showing the test-section, the cylinder and fishing wire supports, and the camera and laser used to acquired to the PIV measurements.

Particle-Image Velocimetry (PIV) was used to measure the velocity fields surrounding the cylinder. The plane at the mid-span of the cylinder, normal to the cylinder axis, was illuminated using an Nd:Yag laser, as shown in Figure 2, and pairs of images were acquired at 200 Hz using a CMOS camera. Silver-coated hollow glass spheres with an average diameter of 10 μm were used to seed to flow. A three-pass cross-correlation scheme with 50% window overlap was used to estimate the velocity fields, which had a final resolution of 18 vectors per cylinder diameter in both the transverse and streamwise directions. The measurement domain spanned the range $x/D = -1.4$ to 4.2 and $y/D = -1.65$ to 1.55, in the streamwise and transverse directions, respectively, with the origin fixed at the mean cylinder position. For each reduced velocity examined, 1000 velocity fields were measured at a sampling rate of 200 Hz. This corresponded to approximately 120 cylinder oscillations per measurement set. The variation in the frequency of traverse velocity fluctuations in the wake, f_w, prior to the onset of VIV was used to calculate the Strouhal number, $St = 0.2$.

The cylinder position was determined directly from the PIV images using a template matching algorithm. The method was found to be accurate to within 0.4 pixels (0.2% of the cylinder diameter).[24] The resulting displacement signals were band-pass filtered between 10 Hz and 40 Hz to remove the effects of noise and any low-frequency variations which were not associated with VIV. The mean peak height of the displacement signal was used to measure the vibration amplitude and the dominant vibration frequency was found from the peak of the power-spectral-density of the signal. This was assumed to be accurate to within 0.78 Hz (0.33% of f_n), which was the resolution of the spectra.

The cylinder displacement signals and velocity fields were measured at 16 freestream velocities in the range $U_0 = 0.1$–0.76 m/s, which corresponded to a Reynolds number range of $Re = U_0 D/\nu$ (where ν is the kinematic viscosity of water) of 740–5400, and a reduced velocity range of $U_r St/f^* = 0.126$–0.714. A settling time of at least 10 min was allowed between adjusting the flow rate and acquiring the PIV measurements. After this period, the PIV system was elevated and a series of measurements were acquired eight diameters upstream of the cylinder in order to measure the freestream velocity; the system was then lowered to its original position and measurements were acquired from the cylinder wake.

In order to clearly identify the vortex-shedding process and the dominant wake mode, the velocity measurements were phase-averaged. As vortex-shedding does not always occur at f_x, it was not possible to phase-average with respect to the cylinder displacement, as is common in transverse VIV studies. Instead, the traverse velocity signal measured at various points in the wake were used as a reference signal, depending on which wake mode was dominant. The vorticity fields were calculated from phase-averaged velocity fields using the least-squares method.

A. Lagrangian analysis

The fluid transport within the wake was studied by numerically advecting passive tracers (with zero size and mass) through the velocity fields using a fourth-order Runge-Kutta scheme and calculating the flow map

$$\phi(\mathbf{x}, t, t_0) = \mathbf{x}(t, t_0, \mathbf{x_0}), \tag{1}$$

which defines the dynamic position of tracers that had an initial distribution $\mathbf{x_0}$ at time t_0. The velocity fields were seeded with tracers with an initial resolution twice that of the velocity vectors (i.e., 36 vectors per cylinder diameter) and the flow map was calculated for both forward- and backward-time. The latter is performed by reversing the flow (i.e., changing the sign of velocity vectors) and allowing the tracers to travel backwards.

Lagrangian Coherent Structures (LCSs) are material lines or surfaces which separate qualitatively distinct regions of the flow and are capable of revealing the underlying patterns in complex flows.[12,39,40] Ridges in the Finite-Time Lyapunov Exponent (FTLE) fields are often used to identify the LCSs; the fields are defined as

$$\sigma_f(\mathbf{x}, t, t_0) = \frac{1}{|t - t_0|} \log \sqrt{\lambda_{\max}}, \tag{2}$$

where $\lambda_{\max}$ is the largest eigenvalue of

$$(\nabla\phi(\mathbf{x}))^{\top}(\nabla\phi(\mathbf{x})). \qquad (3)$$

This is mathematically equivalent to the rate of separation of particles,[12] such that the maximum rate of separation of two particles at point $\mathbf{x}$ with time is proportional to $e^{(\sigma_f(\mathbf{x})(t-t_0))}$. When the FTLE field is calculated in forward-time (i.e., $t > t_0$), the fields are denoted σ_f^+ (where the superscript "+" indicates a forward-time calculation), and regions of high σ_f^+ correspond to points where fluid particles are rapidly moving away from and tend to coincide with *repelling* structures within the flow. Similarly in backward-time calculations, regions of high σ_f^- (where the "−" superscript indicates that the property is calculated in backward-time) correspond to points that fluid moves towards over the period (t to t_0) and therefore tend to represent *attracting* structures.

The FTLE fields in forward- and backward-time were calculated from the phase-averaged velocity fields by allowing the tracers to advect over five wake cycles, i.e., the integration time was $|t - t_0| = 5/f_w$. The FTLE fields were qualitatively similar to those computed over shorter intervals, but the relatively long integration time of $5/f_w$ allowed the complex patterns in the near wake to be fully captured. In most cases outside the recirculation zone, the fluid tracers left the PIV domain before this time, and the FTLE field at this point was calculated based on the time at which the local tracers left the domain.

III. RESULTS

A. Amplitude response

The amplitude response of the cylinder is shown in Figure 3(a) as a function of reduced velocity. The response regime is dominated by two branches, separated by a low amplitude region at $U_r St/f^* \approx 0.5$, in agreement with previous studies.[23,24,33,34] The symbol colours denote the dominant wake mode observed in the PIV fields at each reduced velocity; the A-II mode occurs when the amplitude is very low; both the A-II and S-I modes occur in the first response branch, with unsteady switching between the modes occurring near the peak of the branch;[29] and the SA and A-IV modes are dominant than the second response branch.
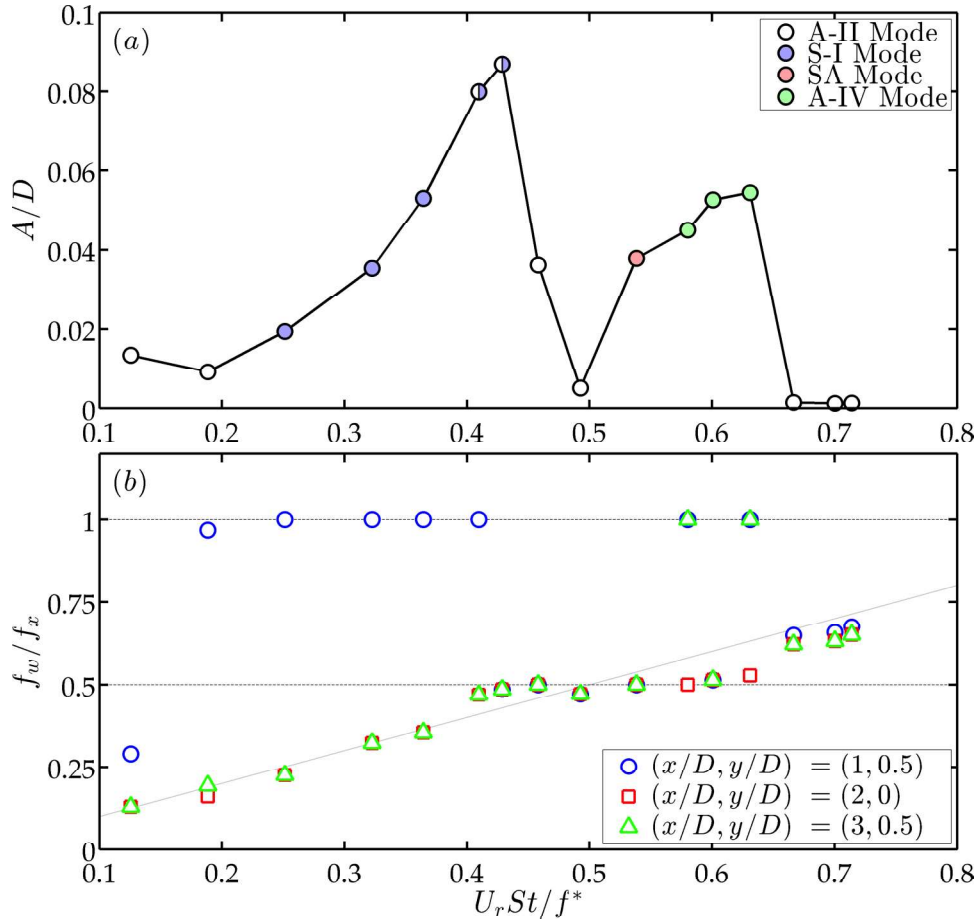
Figure 3(b) shows the dominant frequency of transverse velocity fluctuations at various points in the wake. The velocity signals indicate that lock-in occurs throughout both response branches ($U_r St/f^* \approx 0.2$–0.65) with the velocity fluctuations at some point in the wake locking-in to either $f_x/2$ and f_x. This phenomenon is not identical throughout this range. In the first branch symmetric shedding causes the velocity fluctuations close to the cylinder ($x/D = 1$) to occur at the cylinder vibration frequency, but downstream the vortices rearrange into an alternate pattern causing the velocity fluctuations to occur at the Strouhal frequency.[29] Similarly, when the A-IV modes occurs in the second branch the velocity fluctuations at $(x/D, y/D) = (3, 0.5)$ contain peaks at both $f_x/2$ and f_x; the super-harmonic frequency component at f_x is likely to be caused by the doubling in the number of vortices shed per wake cycle. However, the velocity signals measured at $(x/D, y/D) = (2, 0)$ all have a dominant frequency of $f_x/2$ when this mode is present.

The phase-averaged vorticity fields and FTLE fields for each mode were analysed in detail at a sample reduced velocity, as listed in Table I. Based on the data in Figure 3, different reference signals were used in the phase-averaging process depending on which mode was dominant (also indicated in Table I). The results for each mode are discussed in Subsections III B–III E.

B. A-II mode

Figure 4 shows the vorticity and backward- and forward-time FTLE fields computed at $U_r St/f^* = 0.126$, while the A-II mode occurred. The amplitude response at this reduced velocity is very low ($A/D = 0.013$) and the wake is similar to the von Kármán vortex street observed behind stationary cylinders. The shear layers on either sides of the cylinder extend far into the wake before rolling up to form vortices at $x/D \approx 2$. This can be seen in Figures 4(a)-4(d), where the shear layers at $y/D \pm 0.5$ begin to form concentrated circular patches of vorticity in this region. It can also

Q2

PROOF COPY [15-1670A] 022604PHF

000000-7   N. Cagney and S. Balabani   Phys. Fluids **28**, 000000 (2016)

FIG. 3. Amplitude response (a) and dominant frequency of velocity fluctuations at various points in the wake (b), as a function of reduced velocity. The dashed line in (b) indicates the Strouhal frequency, while the symbol colours in (a) indicate the dominant wake mode: A-II (white); S-I (blue); SA (red); and A-I (green). Symbols with two colours indicate the presence of mode switching.

been seen in the backward-time FTLE fields (Figures 4(e)-4(h)), where thin ridges of σ_f^- extend downstream from the cylinder (in the same positions occupied by the shear layers), before rolling up to form spirals at the same point at which the vortices become apparent in the vorticity fields. An example of this roll up/vortex formation can be seen in the upper shear layer in Figures 4(c) and 4(d) at $x/D \approx 1.5$–2.5, where a circular patch of negative (clockwise rotating) vorticity has formed, and the σ_f^- ridge has rolled up to form a clockwise spiral at the same point (Figures 4(g) and 4(h)). It is apparent that the vortices seen in the ω_z fields coincide with rolled up spiral-shaped σ_f^- ridges, and the vortex formation process is analogous to the roll up phenomenon in the backward-time FTLE fields.

TABLE I. Sample reduced velocities examined and the point in the wake at which the reference signal was extracted for each wake mode.

Mode	Sample $U_r St/f^*$	Reference signal (x/D,y/D)
A-II	0.126	(3,0.5)
S-I	0.365	(1,0.5)
SA	0.538	(3,0.5)
A-IV	0.58	(2,0)

PROOF COPY [15-1670A] 022604PHF

000000-8   N. Cagney and S. Balabani   Phys. Fluids **28**, 000000 (2016)
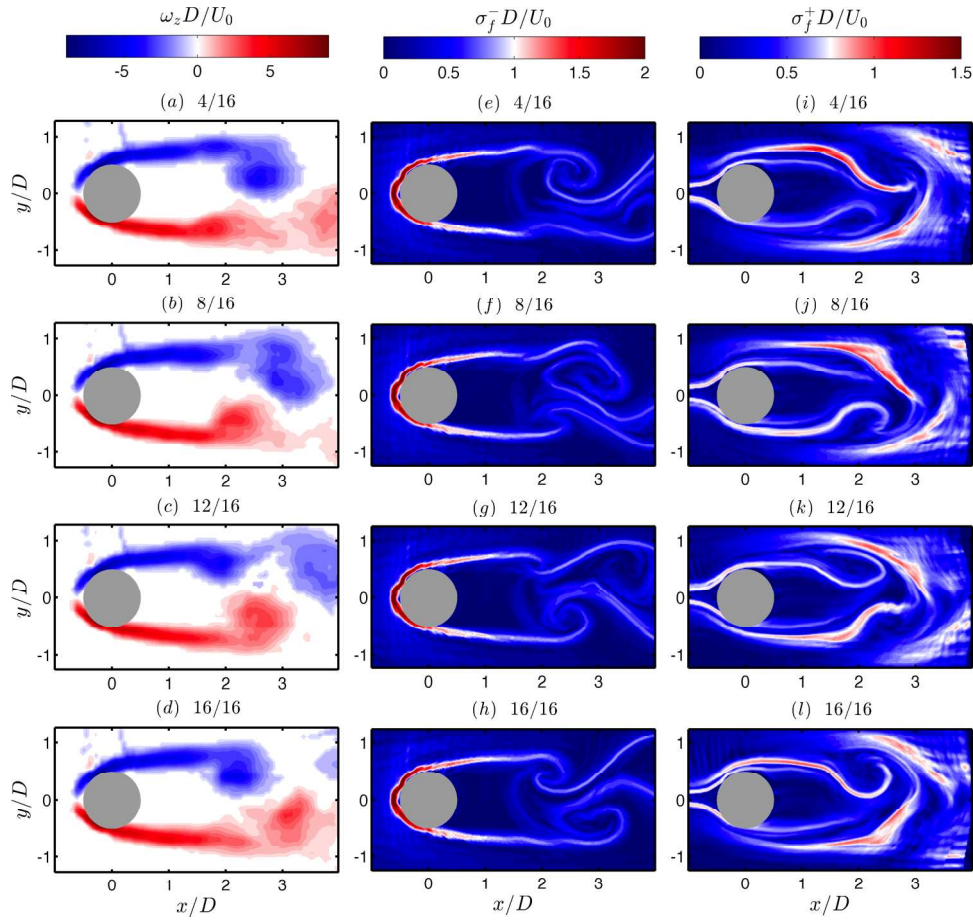

FIG. 4. Phase-averaged vorticity fields (a)-(d) and the Finite-Time Lyapunov Exponents calculated in backward- (e)-(h) and forward-time (i)-(l), at $U_r.St/f^* = 0.126$, while the A-II mode was present. The fields in each row were computed at the same phase in the shedding cycle.

The vortex-shedding process is not as immediately clear in the forward-time FTLE (Figures 4(i)-4(l)). There are two ridges of high σ_f^+ extending from the cylinder in roughly the same position as the shear layers, which also roll up in the wake. However, unlike the ridges in the backward-time FTLE fields, the σ_f^+ ridges appear to roll up to *surround* the newly formed vortices, e.g., at $(x/D, y/D) = (2, -0.5)$ in Figure 4(j). This σ_f^+ ridge has rolled up in an anti-clockwise manner to surround the clockwise rotating vortex as it forms, i.e., the opposite roll up process which we observe in the backward-time fields.

Another interesting feature of the forward-time FTLE fields can be seen in the ridges along the shear layers. While the ridges remain attached to the cylinder throughout the shedding cycle, a strip is "peeled off" each ridge. This can be seen in Figure 4(i), where a single σ_f^+ ridge is attached to the bottom of the cylinder ($y/D = 0$ to -0.5), extending to about $x/D = 2.2$; as the shedding cycle progresses (Figures 4(j) and 4(k)) this layer appears to split in two, with a weaker strip close to the wake centre line remaining attached to the cylinder; by the time the shedding cycle is almost complete (Figure 4(l)), the σ_f^+ ridge has completely split into two separate strips, with a stronger ridge (further from the wake centreline) being cut off from the cylinder and beginning to move downstream.

Finally, two σ_f^+ ridges extend upstream from the front of the cylinder. These features were also observed in previous studies of flow around cylinders[42] and convecting vortex rings,[43] and represent the boundary between regions which are quickly swept downstream and fluid which interacts with

the viscous boundary layer surrounding the cylinder. These upstream ridges were observed in the σ_f^+ fields computed for each mode.

C. SA mode

The SA mode is a special case of the A-II mode, in which the vortices are formed very close to the cylinder and remain close to the wake centreline as they convect downstream. These features can be seen in Figure 5 for $U_r St/f^* = 0.538$; patches of strong vorticity are seen forming at the base of the cylinder (Figures 5(b) and 5(d)), while σ_f^- ridges roll up at the same points (Figures 5(f) and 5(h)). The σ_f^- ridges trace beautiful arcs in the wake, showing the positions of the convecting vortices and the shear layers which connect each vortex. The fields are similar to the dye flow visualisation images of Van Dyke.[1]

The forward-time fields also reveal some interesting features. The peel off process is again observed; a curved arc of high σ_f^+ surrounds much of the cylinder and near wake in Figure 5(i), and as the shedding progress continues a strip is peeled off and moves downstream (e.g., at $x/D \approx 1.75$ in Figure 5(k)). A shed σ_f^+ ridge is visible in each of the forward-time FTLE fields in the range $x/D \approx 1.5$–2.5. They tend to lie perpendicular to the σ_f^- ridges and between the positive and negative vortices in the ω_z fields (Figures 5(a)-5(d)). This, along with the fields presented for the A-II mode, suggests that the forward-time FTLE fields separate the regions in which the vortices form from the surrounding flow. For example, in Figures 5(i)-5(l) the σ_f^+ ridges enclose the vortex
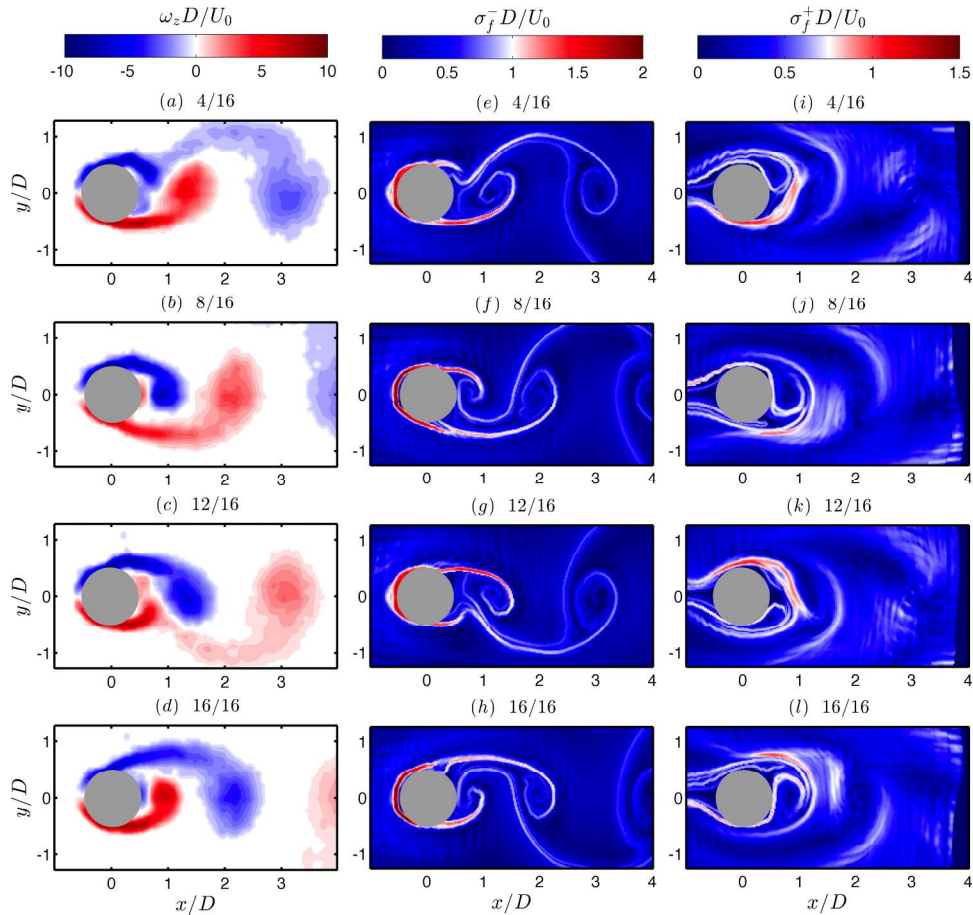
FIG. 5. Phase-averaged vorticity fields (a)-(d) and the finite-time Lyapunov exponents calculated in backward- (e)-(h) and forward-time (i)-(l), at $U_r St/f^* = 0.538$, while the SA mode was present. The fields in each row were computed at the same phase in the shedding cycle.

PROOF COPY [15-1670A] 022604PHF

000000-10   N. Cagney and S. Balabani   Phys. Fluids **28**, 000000 (2016)

formation region at the base of the cylinder throughout the shedding cycle, separating it from the   312
ambient flow and the downstream wake.   313

D. A-IV mode

Figure 6 shows the phase-averaged vorticity and FTLE fields computed at $U_r St/f^* = 0.58$,   315
while the A-IV mode was dominant in the wake. The vorticity patterns are slightly disorganised   316
compared to the other wake modes shown, which is a result of the increased unsteadiness in the   317
vortex-shedding process. The increased number of vortices shed per cycle also means that peak   318
vorticity in each vortex is lower, and they are therefore less clearly distinguishable.   319

However, the shedding of vortex pairs is still visible; positive and negative vortices can be seen   320
convecting downstream as a pair in Figures 6(b) and 6(d) at $x/D = 2$–3. The shed vortex pairs are   321
too weak to be apparent in the FTLE fields (Figures 6(e)-6(l)), but the roll up of vortices in the   322
near wake is clear. Two vortices can be seen in the near wake in Figure 6(h), with a large σ_f^- spiral   323
slightly further downstream ($x/D \approx 1$) on the lower surface. In the following stage of the shedding   324
cycle (Figure 6(e)) the lower σ_f^- spiral has been shed and is no longer visible (although it is apparent   325
at $x/D \approx 2.25$ in the corresponding vorticity field in Figure 6(a)), and a new vortex is starting to   326
form in the same location ($x/D \approx 0.75$). The backward-time FTLE fields reveal the dynamics of   327
the vortex shedding process in the near wake in greater detail than is apparent from the slightly   328
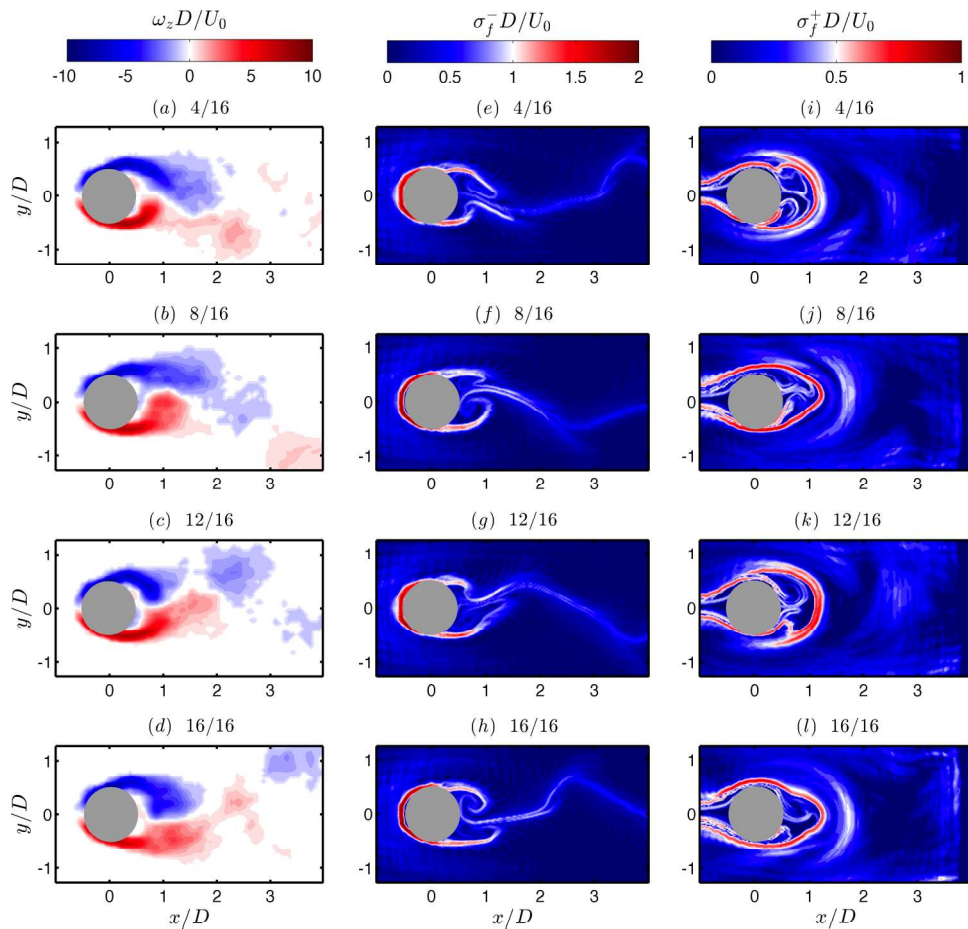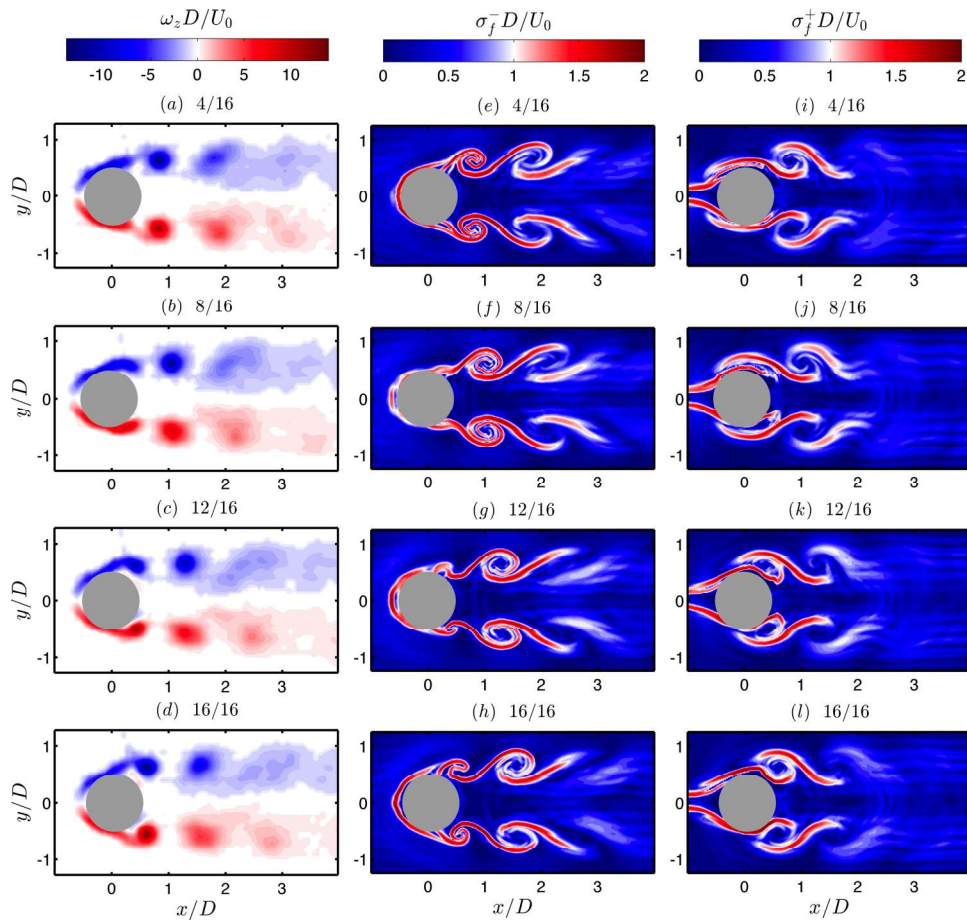disorganised vorticity fields alone.   329

FIG. 6. Phase-averaged vorticity fields (a)-(d) and the Finite-Time Lyapunov Exponents calculated in backward- (e)-(h) and   330
forward-time (i)-(l), at $U_r St/f^* = 0.58$, while the A-II mode was present. The fields in each row were computed at the same   331
phase in the shedding cycle.   332

PROOF COPY [15-1670A] 022604PHF

000000-11   N. Cagney and S. Balabani   Phys. Fluids **28**, 000000 (2016)

The forward-time FTLE fields are shown in Figures 6(i)-6(l). As in the backward-time case, the shed vortices are not visible downstream, although the σ_f^+ fields show strong ridges close to the cylinder. The peel off process is again apparent; however, in this case the σ_f^+ ridge that remains attached to the cylinder appears to enclose the entire near wake region and is connected to both the upper and lower surfaces of the cylinder (e.g., in Figure 6(l)).

The shed strip of the σ_f^+ ridge appears to separate the like-signed vortices which are shed sequentially, for example, the weak ridge at $x/D \approx 1.75$ in Figure 6(l) lies between the positive vortex at $x/D \approx 2.25$ and the newly formed positive vortex at $x/D \approx 1.25$ in Figure 6(d). Therefore, while the A-IV mode occurs, the forward-time FTLE ridges separate the vortex pairs rather than the individual shed vortices, as in other modes.

E. S-I mode

The symmetric shedding mode is unique to streamwise oscillations/excitation[26] and can occur for a wide range of streamwise excitation amplitudes and frequencies.[17] The symmetric nature of the wake is clear in both the phase-averaged vorticity and FTLE fields in Figure 7. The symmetric arrangement of vortices is unstable and rearranges into an alternate pattern downstream;[28,29] the phase-averaging process cancels out these alternate patterns in the velocity fields and no structures are apparent for $x/D \gtrsim 3$ in any of the fields in Figure 7.

FIG. 7. Phase-averaged vorticity fields (a)-(d) and the finite-time Lyapunov exponents calculated in backward- (e)-(h) and forward-time (i)-(l), at $U_r St/f^* = 0.365$, while the S-I mode was present. The fields in each row were computed at the same phase in the shedding cycle.

The vortices formed have a clear circular shape (Figures 7(a)-7(d)) and coincide with "voids" in the forward-time FTLE fields (Figures 7(i)-7(l)), with σ_f^+ ridges rolling up to enclose the regions in which the vortices lies. These regions also coincide with rolled up spirals in the σ_f^- fields (Figures 7(e)-7(h)), as seen in the other wake modes.

The "wake breathing" process has been studied by a number of researchers[17,24,26,28,29,44] since the early flow visualisation study of Aguirre,[23] and the high spatial resolution of the FTLE fields allows this phenomenon to be examined in much greater detail. In particular, we can examine the near-wake processes associated with vortex-formation and shedding which control the overall structures of the fields shown in Figure 7. Figure 8 shows the phase-averaged vorticity fields in the near wake throughout the cylinder oscillation cycle, along with the ridges in the backward- and forward-time FTLE fields and the phase-averaged cylinder position. For the sake of the current discussion, the FTLE ridges are here taken to be all the points where $\sigma_f^- D/U_0 \geqslant 1.25$ and $\sigma_f^+ D/U_0 \geqslant 1.25$. A video showing the periodic roll-up of the shear layers and the FTLE ridges in the near wake region as the cylinder vibrates is provided in the supplementary material.[49]

As the cylinder is in its peak downstream position (Figure 8(a)), a counter-clockwise rotating vortex is present at $x/D \approx 0.75$, which can be identified by a patch of positive vorticity and a σ_f^- spiral (light blue region). This vortex lies in an eye-shaped gap between successive σ_f^+ ridges (dark blue).

The cylinder begins to move upstream, which causes the vortex to separate from the cylinder surface, and by the time the cylinder is passing through its mean position (Figure 8(c)), the cylinder and shed vortex are only connected by a thin strip of vorticity (not visible in the figure) and a narrow σ_f^- ridge. The separation between the cylinder and the vortex causes the σ_f^- ridge connecting them to become elongated, and as the cylinder reaches its peak upstream position (Figure 8(e)) this ridge begins to roll up, marking the onset of the formation of a new vortex. This can also be seen by the growth of a region of positive vorticity at this location. The cylinder oscillation cycle continues, and as the cylinder moves downstream again the vortex grows in strength and a σ_f^- spiral gradually develops on top of this vorticity patch (Figures 8(f)-8(h)). By the time this vortex is shed (Figure 8(c)) the spiral has developed a fine-scale structure, with the radial separation between ridges in the spiral approaching the spatial resolution of the PIV fields (i.e., $0.055D$).

The forward-time FTLE fields also provide insight into the vortex-formation process. When the cylinder is in its peak downstream position (Figure 8(a)) a σ_f^+ ridge lies along the cylinder surface. As the cylinder moves upstream and sheds its vortex (Figures 8(b) and 8(c)), the σ_f^+ ridge undergoes peel off, with a strong ridge being shed into the wake (moving with the shed vortex) and a thinner strip remaining in contact with the cylinder. There are now two roughly parallel σ_f^+ ridges which separate as the cylinder continues to move upstream and the stronger ridge is shed into the wake (Figures 8(c)-8(e)), forming an eye-shaped void (Figures 8(e)-8(h)). Comparison to the vorticity fields in the same figure indicates that these σ_f^+ ridges are forming a "vortex cell," in which the new vortex forms. There is little vorticity at the cylinder surface before the cell forms (Figures 8(a)-8(h)), and the initial peel off process and the separation of the ridges (Figures 8(b) and 8(c)) coincide with the growth of the patch of positive vorticity at the cylinder surface within the vortex cell.

The FTLE fields reveal an organised structure of the flow, as shown in Figure 9. The flow can be roughly divided into three regions; the "ambient flow" outside of the wake, the "turbulent wake" between the trains of vortices on either sides of the wake centreline, and the vortex cells which are occupied by vortices that form in the near wake and dissipate downstream. The vortex cells will move downstream at the convective velocity of the vortices. The role of the FTLE fields in identifying qualitative boundaries within the wake and revealing the underlying flow structure is similar to the "skeleton" of the flow presented by Mathur et al.[40] for freestream turbulence.

IV. MIXING IN THE WAKE

The Lagrangian analysis can also be used to study the mixing dynamics in the wake, following a similar approach to that of Crimaldi and Kawakami[9,10] who studied the wake of a stationary
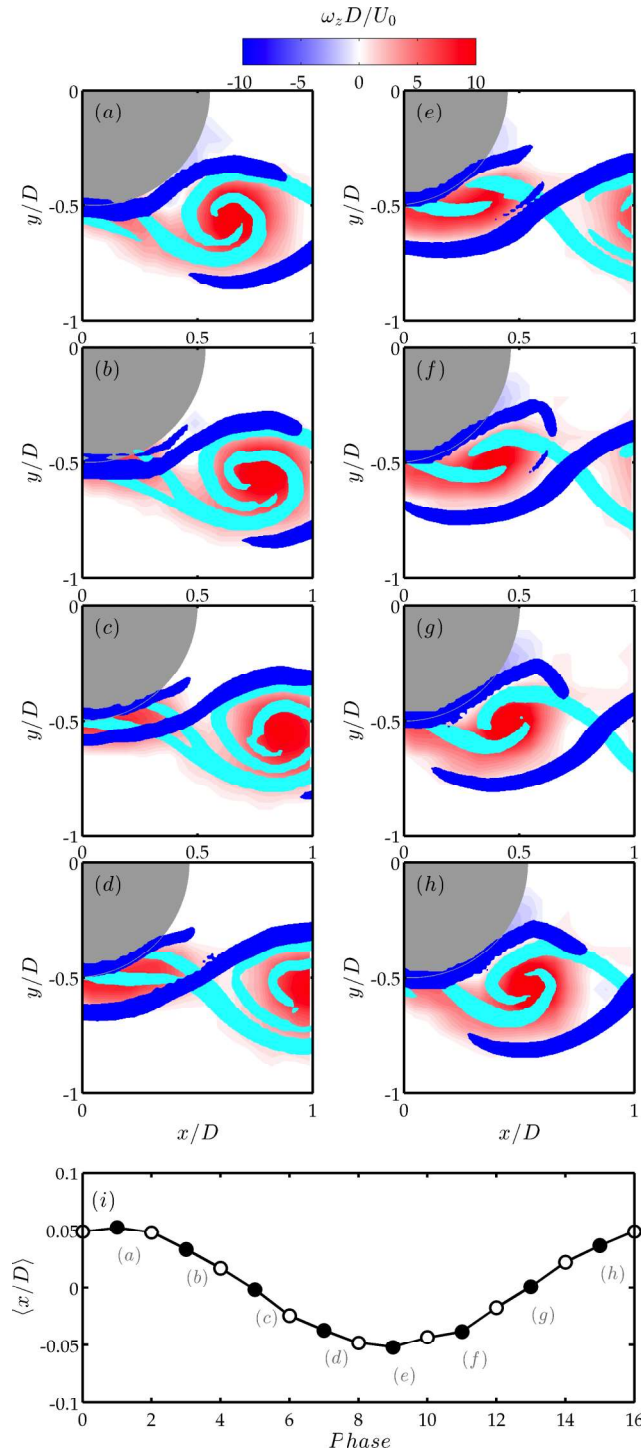
FIG. 8. Phase-averaged vorticity fields (a)-(h) along with the ridges in the backward- and forward-time FTLE fields (light and dark blue, respectively), at $U_r St/f^* = 0.365$. The ridges were defined as regions where $\sigma_f^- D/U_0 \geqslant 1.25$ and $\sigma_f^+ D/U_0 \geqslant 1.25$. The corresponding phase-averaged cylinder position is shown in (j).

cylinder. The problem of mixing in the wake is relevant to the dispersion of effluent or pollutants in rivers and coastal regions. Turbulent mixing is required to reduce the concentration of effluent in the water to safe levels; the presence of reeds and other vegetation (or purposely inserted structures susceptible to VIVs[45]) will result in vortex-shedding which may increase the rate of mixing and

PROOF COPY [15-1670A] 022604PHF

000000-14   N. Cagney and S. Balabani   Phys. Fluids **28**, 000000 (2016)
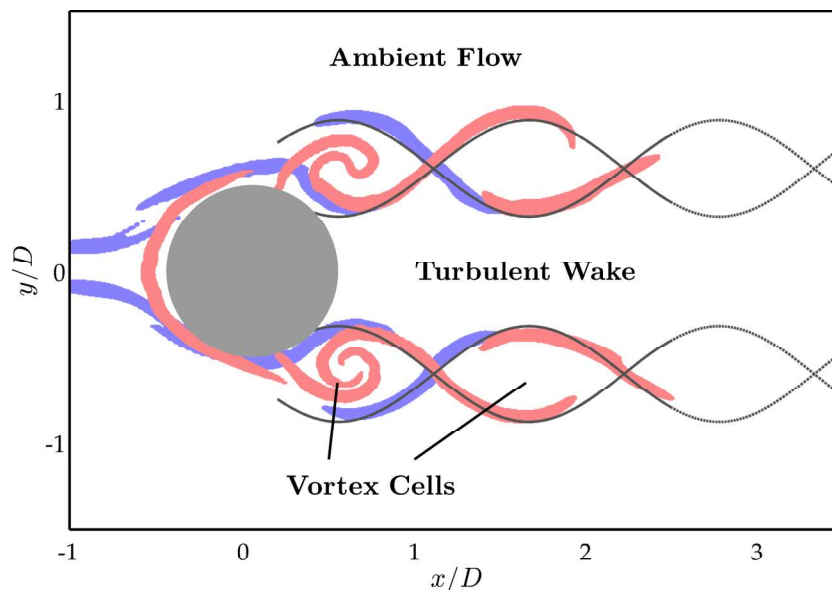
FIG. 9. Decomposition of the S-I wake into three qualitative regions; the ambient region outside of the wake, the turbulent wake and the vortex cells. The red and blue regions are defined by areas in which $\sigma_f^- D/U_0 \geqslant 1.25$ and $\sigma_f^+ D/U_0 \geqslant 1.25$, respectively, and the grey lines show the approximately boundaries of the vortex cells. The FTLE fields were acquired at $U_r St/f^* = 0.365$, and correspond to the fields shown in Figure 8(a).

dispersion and decrease the region of the river with dangerously high contaminant concentration. If the vegetation (which can be approximated as a cylinder) or solid structures are subject to wave loading from wind or sea waves, this case will be equivalent to a cylinder undergoing streamwise VIV in steady flow. It is also relevant to micro-scale flows in which bluff-bodies are purposely inserted and pulsating flow induced to promote mixing and heat transfer.[46,47] It is therefore of interest to investigate what effect each of the wake modes in streamwise VIV has on the mixing efficiency, and under what conditions streamwise VIV will promote or inhibit mixing.

To examine this, we take the ideal case of two streams entering the PIV domain on either sides of the cylinder, in the region $0.75 \leq |y/D| \leq 1$. Mixing in flows is governed by the Péclet number, $Pe = U_0 D/d$ (where d is the mass diffusivity), which is the ratio of the rates of advection and diffusion. The diffusivity for most common fluids in water is of the order of 10^{-9} m^2/s,[48] which corresponds to $Pe > 7 \times 10^5$ for the experiments presented here. This is sufficiently high so that mixing in the wake occurs almost entirely by advection and the effects of diffusion can be neglected in the current analysis.

Tracers were seeded throughout the PIV domain with the same resolution as the FTLE fields (i.e., 36 particles per cylinder diameter) and advected backwards in time using a fourth-order Runge-Kutta scheme to identify the location at which they entered the PIV domain, which was expressed as the instantaneous concentration fields, $C(x, y, t)$. Points at which the local tracer entering the domain from above the cylinder ($0.75 \leq y/D \leq 1$) were assigned a value of 1; a value of -1 was assigned if the local tracer entered from below the cylinder ($-1 \leq y/D \leq -0.75$) and all other points were set to zero. The concentration field was calculated for every PIV field and the results were averaged (omitting the first 100 fields, to avoid erroneously including the effects of any fields in which there was insufficient time to advect the tracers back to the point at which they entered the PIV domain).

This approach was similar to the "coarse-grain density" method of estimating mixing,[7] in which the tracers are advected forward in time and their concentration in a number of bins is examined. However, the current approach of advecting the tracers backwards in time had some advantages for open flows. It guarantees that C can be evaluated at every point in the flow; this is particularly relevant near regions of high vorticity, which tended to be sparsely populated if the tracers are advected forward in time, and near the base of the cylinder where there is reduced mass
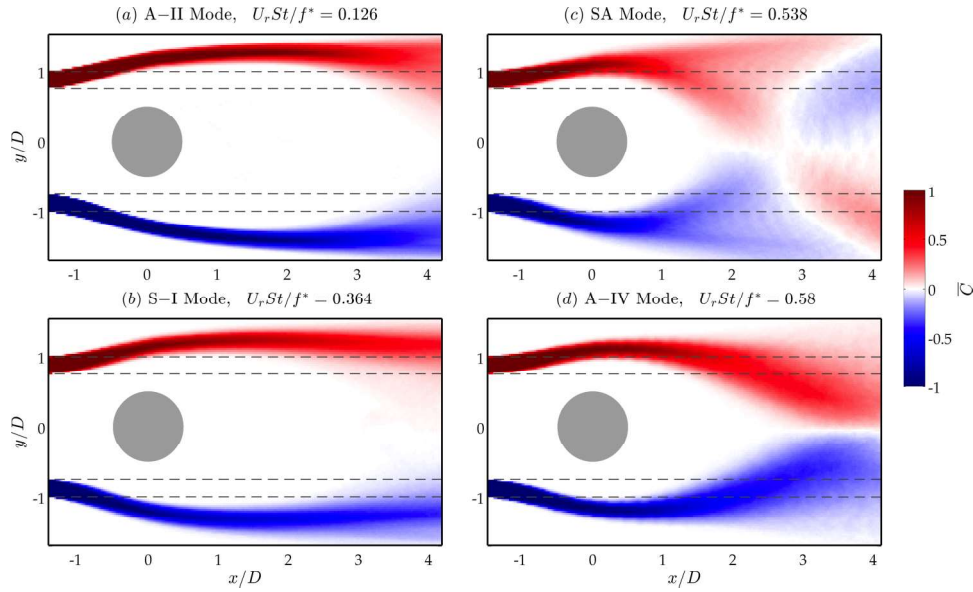
FIG. 10. Mean concentration fields calculated for four wake modes; A-II (a), S-I (b), SA (c), and A-IV (d). The dashed lines show the transverse positions at which the red and blue streams entered the PIV domain, $0.75 \leq |y/D| \leq 1$.

transport in and out of the recirculation region.[5] In addition, it allows for higher resolution of the concentration field relative to the spacing of the tracers, as tracers do not have to be averaged over a bin region.

   The mean concentration fields, $\overline{C}$, for each wake mode are shown in Figure 10, where the red and blue regions correspond to regions where the local tracers originated in the streams above and below the cylinder, respectively. The horizontal dashed lines indicate the transverse positions from which the streams originated. The mean concentration field corresponding to the A-II mode is shown in Figure 10(a) and can be approximated as the $\overline{C}$ field which would be seen behind a stationary cylinder. The two streams enter the domain on the left and spread away from the wake centreline as they pass the cylinder before gradually returning to their original transverse positions. The vortex-shedding and turbulence cause the mean concentration streams to disperse downstream, although for $x/D \lesssim 3$ virtually no material from either streams has moved closer to the centreline from its original position (i.e., $\overline{C} \approx 0$ for all $|y/D| \leq 0.75$). Similarly, little dispersion is observed when the S-I mode occurs (Figure 10(b)), with the streams marginally less dispersed at the downstream boundary of the PIV domain compared to the A-II case.

   In contrast, very strong cross-wake mixing is seen when the SA mode dominates (Figure 10(c)). Here, the tendency for vortices to form at the cylinder base and remain close to the wake centreline causes the streams in the mean concentration field to cross over to the other side of the wake at $x/D \approx 2.75$, where the averaging process results in a mean value close to zero. At the point where the fluid leaves the PIV domain at $x/D = 4.2$, the streams in the $\overline{C}$ field have completely switched sides and the width of each stream is significantly larger than that seen for the A-II or S-I modes, indicating greater mixing and dispersion.

   Figure 10(d) shows that mixing is also enhanced when the A-IV mode is present (although not to the same extent as seen for the SA mode), with the streams becoming wider downstream and meeting at the wake centreline at $x/D \approx 3$–4.

   The mixing characteristics of each mode can be directly compared by examining the transverse profiles of the concentration fields at a given location in the wake. To remove the effect of tracers from either sides of the cylinder "averaging out" in the $\overline{C}$ fields, as occurred in the A-IV and SA fields, only the tracers which originated below the cylinder ($y/D < 0$) were averaged to yield $\overline{C^-}$; this corresponds to the mean concentration of the blue streams in Figure 10. The profiles were calculated for a range of different initial positions of the streams.
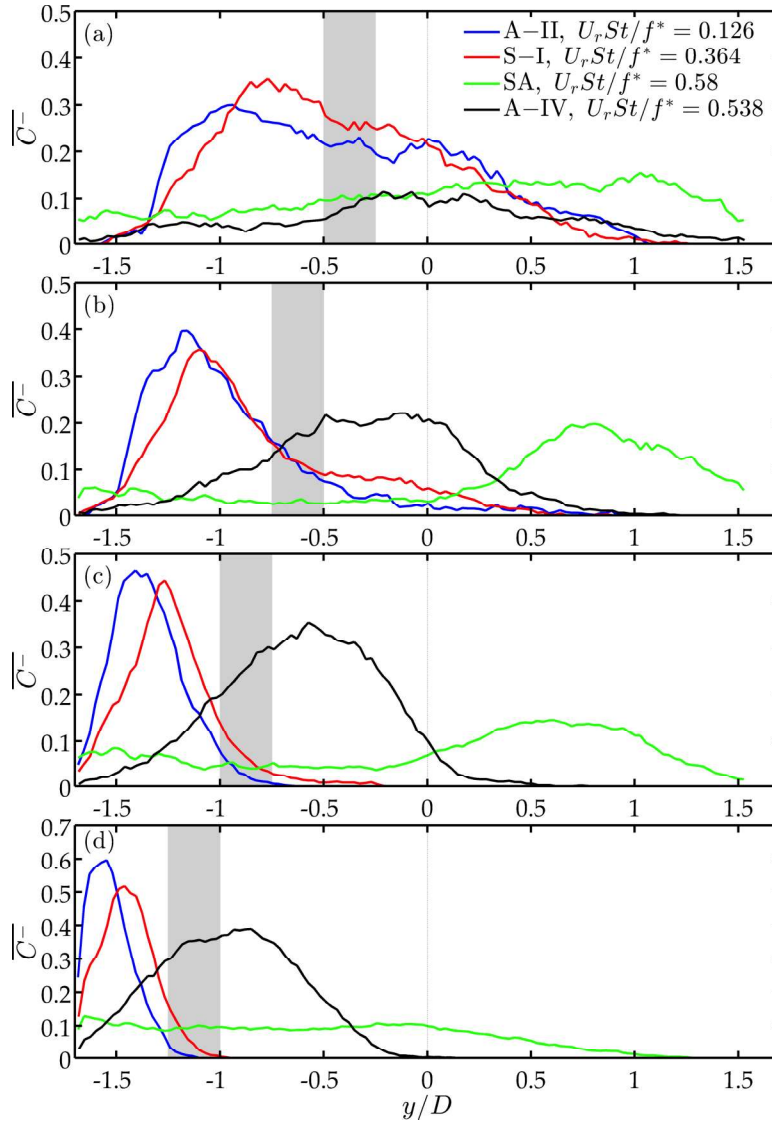
FIG. 11. Transverse profiles at $x/D = 3.5$ of the mean concentration of the tracers entering the PIV domain at $y/D = -0.25$ to -0.5 (a), $y/D = -0.5$ to -0.75 (b), $y/D = -0.75$ to -1 (c), and $y/D = -1$ to -1.25 (d). The shaded regions represent the initial position of the stream as it enters the PIV domain.

Figure 11(c) shows the profiles of $\overline{C^-}$ at $x/D = 3.5$ for the streams entering the domain at $-0.75 \leq y/D \leq -1$, for each of the wake modes. The area underneath each curve will not be the same (as it will depend on the variation in the streamwise velocity component and the flux through the sides of the PIV domain); however, the widths of the peaks in the $\overline{C^-}$ profiles provide a measure of the dispersion of the streams caused by the wake dynamics.

The profiles for the A-II and S-I modes are very similar, with the latter profile occurring slightly closer to the wake centreline. The widths of both peaks are approximately the same, indicating that the two modes do not induce significantly different magnitudes of cross-wake mixing. In contrast, the peak in the profile for the A-IV mode is very broad, spanning the range $y/D \approx -1.5$ to 0 and centred at $y/D \approx -0.5$, indicating a dramatic increase in mixing. As was seen in the $\overline{C}$ fields, the profile for the SA mode also indicates very strong mixing; the profile is not characterised by a single pronounced peak but is distributed across the PIV domain, with $\overline{C^-} \gtrsim 0.04$ for most points. There is a wide bulge at $y/D \approx 0.33-1$ (on the opposite side of the wake to the stream's origin) and a small secondary bulge near $y/D \approx -1.5$, which can also be seen in Figure 10(c).

PROOF COPY [15-1670A] 022604PHF

000000-17   N. Cagney and S. Balabani   Phys. Fluids **28**, 000000 (2016)

Figures 11(a), 11(b), and 11(d) show the $\overline{C^-}$ profiles computed for different initial positions of the streams (as indicated by the grey shaded regions). The profiles are slightly different in each case, tending to be more irregular and broad when streams originate close to the centreline and the tracers are more likely to become entrained in the near wake. However, the general trends are clear; when the SA mode occurs, the cross-wake mixing is strong and tracers are dispersed broadly across the wake; the peak in the $\overline{C^-}$ profile is also broad when the A-IV mode occurs; while the S-I and A-II profiles are narrow.

The $\overline{C}$ fields and $\overline{C^-}$ profiles are representative of the time-averaged cross-wake mixing, but they do not provide information on *how* the mixing occurs, or how this process is related to the Lagrangian structures seen in the FTLE fields. To investigate these questions, we examine the case of the streams originating close to the centreline ($0.25 \le |y/D| \le 0.5$) while the SA mode was dominant at $U_r St/f^* = 0.58$. This case was chosen as it exhibited the strongest cross-wake mixing and the mixing process was clearly visible. Figures 12(a)-12(d) shows the C fields calculated from the phase-averaged velocity fields, and the magnitude of the gradient of these fields is shown in Figures 12(e)-12(h). Regions of high $|\nabla C|$ correspond to points at which you would expect to find the strongest mixing if the streams were "active," e.g., streams of reactive chemical agents[5] or in various biological processes such as the fertilisation of marine species.[41] The fields contains regions
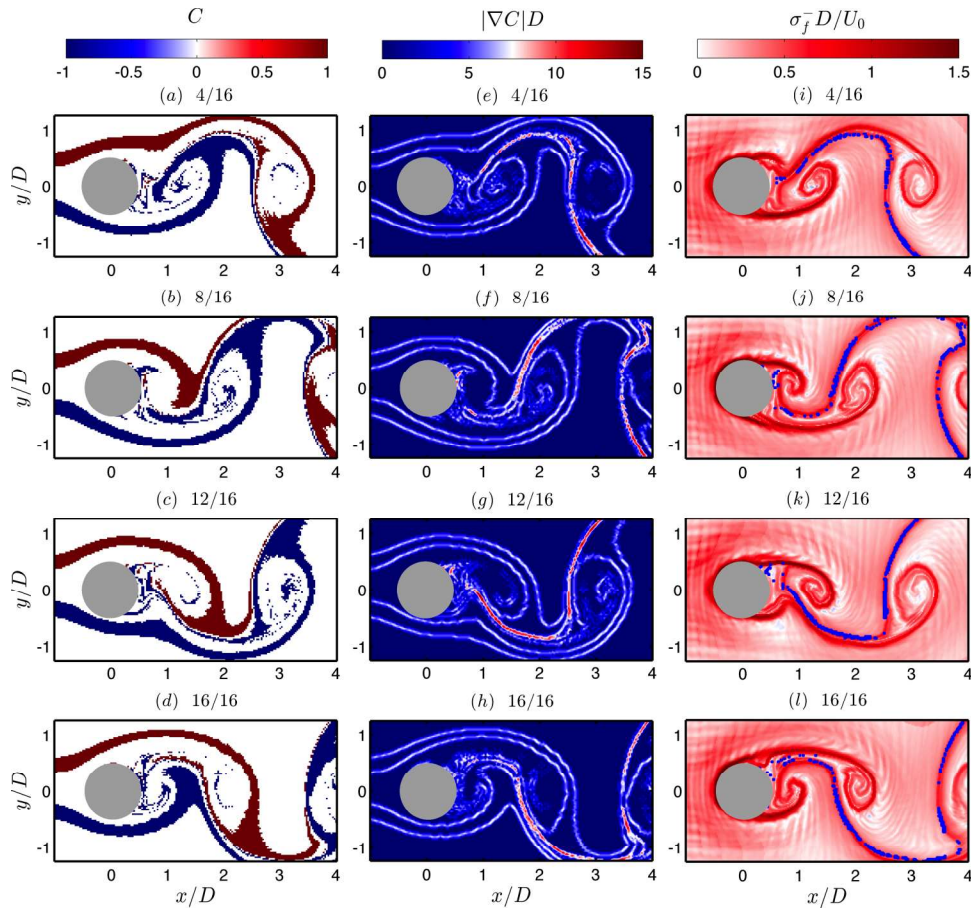
FIG. 12. Concentration fields (a)-(d), the magnitude of the gradient of C (e)-(h) and the Finite-Time Lyapunov Exponents calculated in backward-time (i)-(l), at $U_r St/f^* = 0.58$ while the SA mode was dominant. All fields were computed from the phase-averaged velocity fields, and the fields in each row were computed at the same phase. The blue points in (i)-(l) correspond to locations where the gradient of the concentration field was large, $|\nabla C|D \ge 8.5$, i.e., where the blue and red stream came into close proximity. These points tend to coincide with ridges in the σ_f^- fields.

PROOF COPY [15-1670A] 022604PHF

000000-18   N. Cagney and S. Balabani   Phys. Fluids **28**, 000000 (2016)

where $|\nabla C|D > 8.5$, which correspond to points at which the two fluid streams came very close together, i.e., the separation between the two streams is less than the resolution of the PIV fields.

The points where $|\nabla C|D \geq 8.5$ are indicated on the corresponding σ_f^- fields by the blue points in Figures 12(i)-12(l). The regions of strong mixing tend to occur along ridges in the σ_f^- fields, i.e., the attracting lines in the flow. A similar correspondence between regions of intense mixing and attracting Lagrangian structures has been observed in previous studies.[5,41]

It is clear that mixing is significantly enhanced in the second response branch (where the SA and A-IV modes occur) compared to the case of the near-stationary cylinder, but is not significantly affected by the S-I mode. Symmetric shedding generally occurs when the excitation or cylinder vibration frequency is greater than twice the Strouhal frequency (which is equivalent to $U_r St/f^* < 0.5$).[17,23,26] Therefore, if the frequency of wave loading (or the natural frequency of bodies added to the flow to passively increase mixing by undergoing VIV) is high, i.e.,

$$f > \frac{2St U_0}{D}, \tag{4}$$

the body will not increase the rate of mixing. However, if the frequency is below this value, Figures 10 and 11 indicate that the mixing will be significantly enhanced relative to the stationary cylinder case.

The findings of this study have implications for the design of cooling systems for electronics, where pins are often installed in micro-channels to promote vortex-shedding and thus significantly enhance heat transfer.[46,47] If the flow is forced, Equation (4) provides a criterion by which the forcing frequency can be tuned to optimise mixing.

V. CONCLUSIONS

The velocity fields surrounding a freely oscillating cylinder were measured using particle-image velocimetry and the finite-time Lyapunov exponent fields were calculated in forward- and backward-time. Analysis of the vorticity and FTLE fields measured while the A-II, SA, and A-IV wake modes dominated showed that the roll up of the shear layers to form vortices in the wake coincided with a roll up of the ridges in the backward-time FTLE fields. As the vortices were shed and convected downstream the spirals in the backward-time FTLE fields continued to develop, demonstrating the ability of the FTLE fields to visualise and identify key aspects of the vortex dynamics. The shedding of vortices into the wake coincides with a "peel-off" process in the forward-time FTLE fields, whereby strong ridges which were connected to the cylinder split into two, with the newly formed ridge moving downstream with the shed vortex. The forward-time ridges tended to lie between neighbouring vortices and in the case of the SA and A-IV modes, they were found to separate the near wake (where the vortices were formed) from the surrounding wake.

The FTLE fields and vortex-formation process associated with the S-I mode were analysed in detail. The backward-time fields again identified the roll up of the shear layers as the vortices formed, while the forward-time fields marked the boundaries of "vortex cells," in which new vortices formed. The FTLE fields allowed the flow to be divided into three approximate regions: the ambient flow outside the wake, the turbulent wake between the shed vortices, and the vortex cells.

The mixing efficiency of each of the wake modes was examined by measuring the origin of passive tracers in each instantaneous PIV field and identifying the number of tracers which originated from $0.75 \leq |y/D| \leq 1$ on either sides of the cylinder. The cross-wake mixing was significantly increased in the second response branch when the SA and A-IV modes occurred, but the S-I mode in the first branch was not found to provide an increase relative to the A-II mode observed behind a near-stationary cylinder. Analysis of the concentration fields indicates that the regions of strongest mixing coincide with ridges in the backward-time FTLE fields.

[1] M. Van Dyke, *An Album of Fluid Motion* (Parabolic Press, Stanford, CA, 1982).

[2] D. Etling, "Mesoscale vortex shedding from large islands: A comparison with laboratory experiments of rotating stratified flows," Meteorol. Atmos. Phys. **43**, 145 (1990).

PROOF COPY [15-1670A] 022604PHF

000000-19   N. Cagney and S. Balabani   Phys. Fluids **28**, 000000 (2016)

3 P. Sangrà, A. Pascual, Á. Rodríguez-Santana, F. Machín, E. Mason, J. C. Mcwilliams, J. L. Pelegrí, C. Dong, A. Rubio, J. Arístegui, Á. Marrero-Díaz, A. Hernández-Guerra, A. Martínez-Marrero, and M. Auladell, "The Canary Eddy Corridor: A major pathway for long-lived eddies in the subtropical North Atlantic," Deep Sea Res., Part I **56**, 2100–2114 (2009).

4 C. Jung, T. Tél, and E. Ziemniak, "Application of scattering chaos to particle transport in a hydrodynamic flow," Chaos **3**, 555–568 (1993).

5 T. Tél, G. Károlyi, A. Péntek, I. Scheuring, Z. Toroczkai, C. Grebogi, and J. Kadtke, "Chaotic advection, diffusion, and reactions in open flows," Chaos **10**, 89–98 (2000).

6 S. Wiggins and J. M. Ottino, "Foundations of chaotic mixing," Philos. Trans. R. Soc., A **362**, 937–970 (2004).

7 H. Aref, J. R. Blake, M. Budišić, J. H. E. Cartwright, H. J. H. Clercx, U. Feudel, R. Golestanian, E. Gouillart, Y. Le Guer, G. F. van Heijst, T. Krasnopolskaya, R. S. MacKay, V. V. Meleshko, G. Metcalfe, I. Mezić, A. P. S. de Moura, K. El Omari, O. Piro, M. F. M. Speetjens, R. Sturman, J.-L. Thiffeault, and I. Tuval, "Frontiers of chaotic advection," preprint arXiv:1403.2953 (2014).   Q4

8 M. Sandelescu, E. Hernández-García, C. López, and U. Feudel, "Kinematic studies of transport across and island wake, with application to the Canary islands," Tellus **58A**, 605–615 (2006).

9 J. P. Crimaldi and T. R. Kawakami, "Reaction of initially distant scalars in a cylinder wake," Phys. Fluids **25**, 053604 (2013).

10 J. P. Crimaldi and T. R. Kawakami, "Reaction enhancement in an unsteady obstacle wake: Implications for broadcast spawning and other mixing-limited processes in marine environments," J. Mar. Syst. **143**, 130–137 (2015).

11 J. A. Bourgeois, P. Sattari, and R. J. Martinuzzi, "Coherent vortical and straining structures in the finite wall-mounted square cylinder wake," Int. J. Heat Fluid Flow **35**, 130–140 (2012).

12 S. C. Shadden, F. Lekien, and J. E. Marsden, "Definition and properties of Lagrangian coherent structures from finite-time Lyapunov exponents in two-dimensional aperiodic flows," Physica D **212**, 271–304 (2005).

13 L. Kourentis and E. Konstantinidis, "Uncovering large-scale coherent structures in natural and forced turbulent wakes by combining PIV, POD and FTLE," Exp. Fluids **52**, 749–763 (2012).

14 B. Celik and A. Beskok, "Mixing induced by a transversely oscillating circular cylinder in a straight channel," Phys. Fluids **21**, 073601 (2009).

15 T. L. Morse and C. H. K. Williamson, "Prediction of vortex-induced vibration response by employing controlled motion," J. Fluid Mech. **634**, 5–39 (2009).

16 C. H. K. Williamson and A. Roshko, "Vortex formation in the wake of an oscillating cylinder," J. Fluids Struct. **2**, 355–381 (1988).

17 S. J. Xu, Y. Zhou, and M. H. Wang, "A symmetric binary-vortex street behind a longitudinally oscillating cylinder," J. Fluid Mech. **556**, 27–43 (2006).

18 M. P. Païdoussis, "Real-life experiences with flow-induced vibrations," J. Fluids Struct. **22**, 741–755 (2006).

19 T. Sarpkaya, "A critical review of the intrinisic nature of vortex-induced vibrations," J. Fluids Struct. **19**, 389–447 (2004).

20 C. H. K. Williamson and R. Govardhan, "Vortex-induced vibrations," Annu. Rev. Fluid Mech. **36**, 413–455 (2004).

21 E. Konstantinidis, S. Balabani, and M. Yianneskis, "The effect of flow perturbations on the near wake characteristics of a circular cylinder," J. Fluids Struct. **18**, 367–386 (2003).

22 E. Konstantinidis, S. Balabani, and M. Yianneskis, "The timing of vortex shedding in a cylinder wake imposed by periodic inflow perturbations," J. Fluid Mech. **543**, 45–55 (2005).

23 J. E. Aguirre, "Flow induced, in-line vibrations of a circular cylinder," Ph.D. thesis, Imperial College of Science and Technology, 1977.

24 N. Cagney and S. Balabani, "Wake modes of a cylinder undergoing free streamwise vortex-induced vibrations," J. Fluids Struct. **38**, 127–145 (2013).

25 A. Ongoren and D. Rockwell, "Flow structure from an oscillating cylinder. Part 2. Mode competition in the near wake," J. Fluid Mech. **191**, 225–245 (1988).

26 E. Naudascher, "Flow-induced streamwise vibrations of structures," J. Fluids Struct. **1**, 265–298 (1987).

27 N. Jauvtis and C. H. K. Williamson, "Vortex-induced vibration of a cylinder with two degrees of freedom," J. Fluids Struct. **17**, 1035–1042 (2003).

28 E. Konstantinidis and S. Balabani, "Symmetric vortex shedding in a near wake of a circular cylinder due to streamwise perturbations," J. Fluids Struct. **23**, 1047–1063 (2007).

29 N. Cagney and S. Balabani, "Mode competition in streamwise-only vortex induced vibrations," J. Fluids Struct. **41**, 156–165 (2013).

30 N. Cagney and S. Balabani, "Streamwise vortex-induced vibrations of cylinders with one and two degrees of freedom," J. Fluid Mech. **758**, 702–727 (2014).

31 N. Cagney and S. Balabani, "Fluid forces acting on a cylinder undergoing streamwise vortex-induced vibrations," J. Fluids Struct. **62**, 147–155 (2016).

32 E. Konstantinidis, S. Balabani, and M. Yianneskis, "Bimodal vortex shedding in a perturbed cylinder wake," Phys. Fluids **19**, 011701-1–011701-4 (2007).

33 N. Cagney and S. Balabani, "On multiple manifestations of the second response branch in streamwise vortex- induced vibrations," Phys. Fluids **25**, 1–17 (2013).

34 A. Okajima, A. Nakamura, T. Kosugi, H. Uchida, and R. Tamaki, "Flow-induced in-line oscillation of a circular cylinder," Eur. J. Mech., B **23**, 115–125 (2004).

35 R. Govardhan and C. H. K. Williamson, "Modes of vortex formation and frequency response of a freely vibrating cylinder," J. Fluid Mech. **420**, 85–130 (2000).

36 R. J. Adrian, K. T. Christensen, and Z. C. Liu, "Analysis and interpretation of instantaneous turbulent velocity fields," Exp. Fluids **29**, 275–290 (2000).

37 G. Haller, "An objective definition of a vortex," J. Fluid Mech. **525**, 1–26 (2005).

38 G. A. Rosi, A. M. Walker, and D. E. Rival, "Lagrangian coherent structure identification using a Voronoi tesselation-based networking algorithm," Exp. Fluids **56**, 189 (2015).

[39] G. Haller, "Lagrangian coherent structures," Annu. Rev. Fluid Mech. **47**, 137–161 (2015).

[40] M. Mathur, G. Haller, T. Peacock, J. E. Ruppert-Felsot, and H. L. Swinney, "Uncovering the Lagrangian skeleton of turbulence," Phys. Rev. Lett. **98**, 144502 (2007).

[41] K. R. Pratt, J. D. Meiss, and J. R. Crimaldi, "Reaction enhancement of initially distant scalars by Largrangian coherent structures," Phys. Fluids **27**, 035106 (2015).

[42] J. Kasten, C. Petz, I. Hotz, H. Hege, B. R. Noack, and G. Tadmor, "Lagrangian feature extraction of the cylinder wake," Phys. Fluids **22**, 091108 (2010).

[43] C. O'Farrell and J. O. Dabiri, "Pinch-off of non-axisymmetric vortex rings," J. Fluid Mech. **740**, 61–96 (2014).

[44] C. Barbi, D. P. Favier, C. A. Maresca, and D. P. Telionis, "Vortex shedding and lock-on of a cylinder in oscillatory flow," J. Fluid Mech. **170**, 527–544 (1986).

[45] M. M. Bernitsas, K. Raghavan, Y. Ben-Simon, and E. M. H. Garcia, "VIVACE (vortex induced vibration aquatic clean energy): A new concept in generation of clean and renewable energy from fluid flow," J. Offshore Mech. Arctic Eng. **130**, 1–15 (2008).

[46] A. Renfer, M. K. Tiwari, R. Tiwari, F. Alfieri, T. Brunschwiller, B. Michel, and D. Paulikakos, "Microvortex-enhanced heat transfer in 3D-integrated liquid cooling of electronic chip stacks," Int. J. Heat Mass Transfer **65**, 33–43 (2013).

[47] A. Renfer, M. K. Tiwari, R. Tiwari, T. Brunschwiller, B. Michel, and D. Poulikakos, "Experimental investigation into vortex structure and pressure drop across microcavities in 3D integrated electronics," Exp. Fluids **51**, 731–741 (2011).

[48] E. L. Cussler, *Diffusion: Mass Transfer in Fluid Systems*, 2nd ed. (Cambridge University Press, New York, 1997).

[49] See supplementary material at http://dx.doi.org/10.1063/1.4945784 for a video showing the periodic roll-up of the shear layers and the FTLE ridges in the near wake region as the cylinder vibrates and symmetric vortex-shedding occurs.